Self-assembly of poly(styrene-block-acrylated epoxidized soybean oil) star-brush-like block

copolymers

Fang-Yi Lin, Austin D. Hohmann, Nacú Hernández, Liyang Shen, Hannah

Dietrich, and Eric W. Cochran\*

Department of Chemical and Biological Engineering, Iowa State University, Ames, IA 50011

E-mail: ecochran@iastate.edu

Abstract

Here we report dynamic and thermodynamic aspects of the self-assembly in a series of branched-chain soybean-oil-derived styrenic block copolymers produced *via* reversible addition-fragmentation chain transfer (RAFT) polymerization. These biobased materials display unusual domain expansion which has not been seen in conven-

tional petroleum-based block copolymers. The chain architecture of poly(styrene-b-

acrylated epoxidized soybean oil) (PS-PAESO) block copolymers varies from star-like

to star-brush-like owing to the bulk and multifunctionality of the PAESO repeat unit.

The self-assembly behavior is evaluated through a combination of (ultra) small-angle

X-ray scattering (SAXS), transmission electron microscopy, and dynamic shear rheol-

ogy. Microphase separation in PS-PAESO is kinetically limited due to sluggish chain

dynamics that cannot be thermally accelerated due to interference from crosslinking

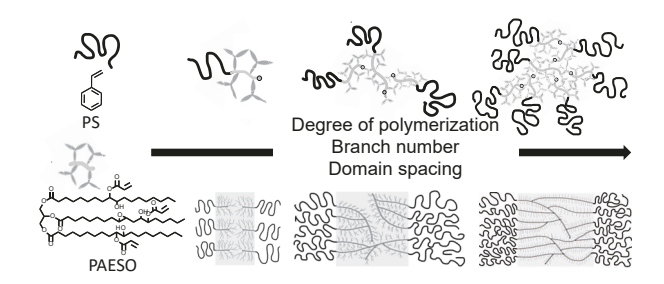
reactions. Selective hydrogenation of the residual PAESO vinyl groups retards but

does not eliminate crosslinking reactions, indicating that transesterification is also at

play. SAXS experiments show that the PS-PAESO domain size scales nearly linearly

1

with number of statistical segments, with structures as large as  $d=155\,\mathrm{nm}$  observed. We believe that domain dilation is related to bulky aliphatic side chains in PAESO domains that extend the primary chain backbone to produce a brush-like conformation. The understanding of the structure-property relationships of these new biobased block copolymers gives insights on the design of novel polymer architectures benefiting new applications.



#### Introduction

Block copolymers, comprised of two or more distinct monomer sequences, are widely known to phase separate at the nanoscale and form different morphologies. Common morphologies in linear AB diblock copolymer systems include lamellae, hexagonally-packed cylinders, body centered spheres, cubic networks (gyroids), orthorhombic networks ( $O^{70}$ ) and close-packed spheres.<sup>1,2</sup> The governing parameters for block copolymer self-assembly are primarily the segregation strength between the different blocks, denoted as Flory-Huggins interaction parameter  $\chi$ , the block composition f, and the molecular weight or number of statistical segments N. Historically, the fundamentals of block copolymer self-assembly were developed with nearly-monodisperse block copolymers, usually synthesized by anionic polymerization. Since anionic polymerization only deals with a certain class of monomers, various synthetic techniques such as controlled radical polymerizations and polycondensation have been adopted to accommodate polymers with manifold functional groups. The dispersity (D) of polymers is inevitably increased with different synthetic techniques involved. With increasing D of polymers,

Leibler and Benoit first predicted in 1981 that the domain spacing expands in homopolymer blends and block copolymers using the random phase approximation. This behavior was later experimentally proven by Lynd and Hillmyer and Noro  $et\ al.^5$  Other simulation predictions on the impact of D on block copolymer self-assembly include the shifts of morphology and order-disorder transitions. Though quantitative discrepancies exist, these shifts were verified experimentally in poly(ethylene-alt-propylene)-b-poly(DL-lactide) and polystyrene-b-polyisoprene (PS-PI) systems.

In addition to linear block copolymers, non-linear block architectures can be designed through various synthetic approaches. For example, star (radial) block copolymers (AB)<sub>n</sub> and miktoarm copolymers (A<sub>m</sub>B<sub>n</sub>) are prepared by adding linking agents to linear block copolymers and/or homopolymers. The linking agents serve as the core of these nonlinear copolymers from which polymer chains branch out as arms. 13 The self-assembly of these non-linear copolymers is governed by the number of arms, along with the composition and molecular weight. 14 Both experimental and simulation 15-17 results indicate that these non-linear copolymer morphologies shift with the numbers of arms. For example, Thomas et al. demonstrated that as the number of arms increases in asymmetric star block copolymers, the morphology changes from hexagonal packed cylinders to the ordered bicontinuous structure. 18,19 The order-disorder transition (ODT) of these star block copolymers is also affected by the number of arms, which is evidenced by the decrease of the segregation strength with increasing number of arms. 20 Besides using linking agents to connect polymers for star block copolymer preparation, another method to synthesize star-like block copolymers is copolymerizing linear homopolymers with multifunctional monomers. 21 Multifunctional monomers, or crosslinkers, are monomers that contain more than one active site that allows polymer chains to branch during polymerization. Instead of branching arms from a single core, this type of block copolymer has multiple branching points distributed stochastically throughout the chain.

The role of crosslinkers in block copolymer self-assembly varies depending on the

thermodynamic and dynamic states in which the crosslinks are formed. When block-selective crosslinks are introduced in the ordered state, the structure is stabilized; for instance block-selective crosslinks can preserve the melt-state morphology in solution. <sup>22</sup> In contrast, if block copolymers are selectively crosslinked in the disordered state, crosslinkers will hinder the phase separation process when approaching the ordered state. For example, Sakurai *et al.* demonstrated that the increase of crosslinker content results in the loss of long range order based on small angle X-ray scattering (SAXS) and transmission electron microscopy (TEM). <sup>23</sup> With the formation of networks by crosslinkers, the crosslinks pin the structure and trap the freely moving blocks from escaping. This crosslinker pinning effect also affects the order-disorder transition. Balsara *et al.* revealed that the order-disorder transition temperature ( $T_{ODT}$ ) increases with increasing crosslink density in crosslinked PS-PI systems. <sup>24–26</sup>

In addition to using a crosslinking agent to prepare non-linear (block) copolymers, bottle-brush block copolymers, another class of non-linear block copolymers, are obtained through grafting polymers  $^{27-29}$  or polymerizing macromonomers with long side chains.  $^{30,31}$  The self-assembly of bottle-brush block copolymers often presents extraordinarily large domain size exceeding  $100 \ nm$ ,  $^{27-31}$  while the domain size of regular linear block copolymers usually falls below  $50 \ nm$  due to the synthetic limitation of the molecular weight. It is revealed that the domain spacing is increased linearly with the degree of polymerization (DP) of the backbone,  $^{28,30}$  which indicates the domain expansion is a result of backbone stretching-out. Moreover, the size of side chains also has a minor impact such that increasing side chain length leads to a slight increase in domain spacing. Besides domain spacing, both experimental and simulation results have shown the lamellae and cylinder morphology of bottle-brush block copolymers by tuning the volume fraction and side chain lengths of different blocks.  $^{32,33}$  These sub-micron patterns show a great potential in applications of optics and filtration fields.  $^{27}$ 

While the aforementioned block copolymers are mainly built from petroleum-based

chemicals, biobased polymers have become increasingly important for both environmental considerations as well as dramatic supply and price fluctuations faced by many petroleumbased feedstocks.<sup>34</sup> The incorporation of biobased monomers has created block copolymers with new and unique architectures that can be used in novel applications. 35 Among these biobased monomers, acrylated epoxidized soybean oil (AESO) has shown to build various architectures including linear, branched and hyperbranched polymers. 36,37 The distinctive PAESO architectures are ascribed to their multi-functional nature and unusually bulky pendent groups. By conjugating rubbery PAESO with other hard-segment blocks, PAESO-based thermoplastic elastomers with various architectures can be obtained. Herein we synthesize polystyrene-*block*-poly(acrylated epoxidized soybean oil) (PS-PAESO) thermoplastic elastomers by extending polystyrene macromonomers with AESO monomers via reversible addition-fragmentation chain transfer (RAFT) polymerization. PS-PAESO has demonstrated its competitiveness toward SBS in bitumen modification. 38,39 The blend of bitumen and PS-PAESO showed a similar or better performance compared to SBSmodified bitumen in terms of complex shear modulus. However, a detailed investigation on the structure-property relationship of PS-PAESO is required. By thoroughly understanding the self-assembly behavior of PS-PAESO, the ability to adjust the performance in applications will be enhanced. At a more fundamental level, the AESO monomer introduces the extent of branching as an adjustable parameter for influencing the self-assembly dynamics and thermodynamics independently of composition and molecular weight.

In this study we synthesize a series of PS-PAESO block copolymers with different molecular weights, compositions, and the branching extent of AESO to investigate their self-assembly and response to thermal treatment. Depending on the branching extent of the PAESO block, the architecture of PS-PAESO varies from linear A-B block copolymers to star-like and star-brush-like block copolymers. In contrast to conventional star block copolymers, branches in PS-PAESO block copolymers extend from multiple points and are statistically distributed. The self-assembly of pre-annealed PS-PAESO is investigated

by SAXS complemented with TEM. The residual acrylic functionality enables selective crosslinking of PAESO domains, which is inevitable during high temperature melt processing or annealing; this phenomenon is also studied from both rheological and morphological aspects. Isochronal testing and master curves are conducted using dynamic shear rheology, while any potential phase change is captured by temperature-dependent SAXS. These findings will support our understanding of this new type of block copolymer self-assembly behavior and thus help researchers design suitable block copolymer architectures in applications.

## **Experimental**

#### **Materials**

Methyl hydroquinone (Sigma-Aldrich), inhibitor remover (Sigma-Aldrich), styrene (Acros), tetrahydrofuran (THF, Fisher), 2-methyl tetrahydrofuran (methyl THF, Sigma-Aldrich), dicumyl peroxide (DCP, Sigma-Aldrich), Eastman 168 non-phthalate plasticizer (P, Eastman), p-toluenesulfonyl hydrazide (tosyl hydrazide, Sigma-Aldrich), and o-xylene (Fisher) were used as received. Soybean oil, epoxidized acrylate (AESO, Sigma-Aldrich) was diluted by methyl THF and passed through the inhibitor remover column before conducting polymerization reactions. Azobisisobutyronitrile (AIBN, Sigma-Aldrich) was recrystallized from methanol. Ethyl(3-oxobutan-2-yl) carbontrithioate (OXCART) was synthesized using procedures described elsewhere. 40

## **Block copolymer synthesis**

The block copolymer was obtained via two-step RAFT polymerization. The first step was the preparation of polystyrene macromonomer with OXCART. For a typical synthesis, styrene (40 g, 0.38 mol), OXCART (0.17 g, 800  $\mu$ mol), and DCP (0.04 g, 160  $\mu$ mol) were

sealed and purged under argon for 15 min in a 100 mL round bottom flask. The reaction was carried out for 8 hrs at 110 °C. The PS macromonomer was diluted in THF and crashed in methanol three times (from THF solution) before further use. The second step was the chain extension of PS macromonomer with AESO. PS macromonomer (7.17 g, 414 mmol), AESO (10 g, 8.33 mmol), AIBN (13.5 mg, 83  $\mu$ mol), and methyl THF (51.51 g, 600 mmol) were sealed and purged under argon for 20 min in a 250 mL round bottom flask. The reaction was carried out for 3.5 hrs at 75 °C. The product was then crashed in methanol three times (from THF solution) followed by three cyclohexane washes. The polymer was then inhibited using 2 wt% methyl hydroquinone via solvent blending. In PS-PAESO/plasticizer blending entries, 20 wt% of Eastman 168 non-phthalate plasticizer (P) was added to PS-PAESO via solvent blending. Plasticized/non-plasticized samples were thermally annealed at 80 °C/ 120°C for five day in vacuum before investigating polymer morphology.

### Selective hydrogenation of block copolymer

The pendent vinyl groups in PS-PAESO were selectively hydrogenated by tosyl hydrazide. <sup>41</sup> PS-PAESO (0.5 g, 211  $\mu$ mol of pendent vinyl groups determined by <sup>1</sup>H NMR), tosyl hydrazide (0.31 g, 1.69 mmol, 8 equiv.), and o-xylene were charged in a two-neck flask and purged under argon for 30 min. The flask was connected to a reflux condenser and a gas bubbler. The reaction was heated up to 80 °C to fully dissolve tosyl hydrazide and then gradually heated to 140 °C to reflux under argon blanket. The reaction was stopped when the evolution of gases ceased. The product was recovered by crashing in methanol three times (from THF solution) to wash out any excess tosyl hydrazide and byproduct.

#### Characterization

 $^1$ H NMR spectra were recorded using a Varian MR-400 spectrometer (400 MHz). The molecular weight distribution as synthesized was characterized by the integrated gel permeation chromatography (GPC) system in chloroform at 1 mL/min. The GPC system consists of 515 HPLC pump (Waters), 717 autosampler (Waters), three PLgel individual pore size GPC columns along with a PLgel guard columns (Agilent), an Optilab T-rEX refractometer (Wyatt), and a dual 270 detector (Malvern) with viscometer and 2-angle light scattering detectors ( $7^{\circ}$ ,  $90^{\circ}$ ). The columns and detectors were calibrated by polystyrene triple detection standards (Malvern) along with a series of polystyrene standards (Scientific polymers) with molecular weights from 570 to 2 M Da. Samples were prepared at 5 mg/mL in chloroform and passed through the 0.45  $\mu$ m PTFE filter.

The glass transition temperature ( $T_g$ ) of block copolymers and homopolymers were recorded by DSC Q2000 (TA instruments). Specimens were sealed in hermetic aluminum pans and subject to three cycles of heating and cooling under nitrogen. The heating and cooling rates were 20  $^{\circ}C/min$  and 10  $^{\circ}C/min$ , respectively. All  $T_g$  values were reported from the second scan after erasing the thermal history of specimens.

The sol-gel fraction and swelling ratio of pre-annealed samples were recorded gravimetrically after soaking in excess toluene. After seven days, the gel part is weighed after blotted dry. The rest of solution was vacuum dried to obtain to sol part weight. The weight-based sol fraction ( $W_{sol}$ ) is the fraction of the sol to the original sample; the weight-based swelling ratio ( $Q_M$ ) is the weight of the blotted dry gel part over the difference between the original sample and the sol part.

Dynamic shear rheology was conducted on ARES-G2 Rheometer (TA instruments) under nitrogen with 8 mm parallel plates. The linear viscoelastic region (LVR) of samples, the range of strain with constant modulus, was determined by strain sweep at different temperatures at 1 rad/s under ca. 0.2 N axial force. Subsequently, temperature-dependent frequency sweep was performed between 1-100 rad/s using the same axial

force within the LVR of the material. Time-temperature superposition (TTS)<sup>42</sup> was applied to generate the master curve for each material. Isochronal testing, the temperature sweep at constant strain and frequency, was conducted from 50 to 250 °C with a heating rate of 10 °C/min under ca. 0.2 N axial force within the LVR of the material at 80°C.

SAXS measurements were conducted at beamline APS 9-ID-C in Argonne national lab and also by in-house Xenocs Xeuss 2.0 SWAXS system. The experiment at APS 9-ID-C beamline was set to a sample-to-detector distance of 546.44 mm and X-ray wavelength ( $\lambda$ ) of 0.5904 Åcollimated by Si(111). Detailed settings can be found elsewhere by Ilavsky et al. <sup>43</sup> Samples were sealed in DSC aluminum hermetic pans, and fixed onto the temperature controlled stage. Data acquisition was conducted from room temperature to approximately 180 °C. Sample was equlibrated at the desired temperature for 300 s followed by an acquisition of 60 s. Data are processed by Indra 2 and Irena macros run on Igor Pro. <sup>44,45</sup> XENOCS Xeuss 2.0 SWAXS system is set with monochromatized X-ray using Cu K $\alpha$  radiation of the wavelength  $\lambda = 1.5406$  Å. Data were collected by Pilatus 1M detector at the sample-to-detector distance of 2514 mm calibrated by silver behenate standard. Samples were sealed between Kapton tape and acquired for a 600 s acquisition.

The real-space morphology of PS-PAESO was imaged by the STEM (JEOL 2100, 200 kV) in Microscopy and NanoImaging Facility at Iowa State University or the STEM (FEI Tecnai G2-F20, 200 kV) in Sensitive Instrument Facility at Ames National Lab. The specimens were sectioned at -70 °C by the cryo-ultramicrotome (Leica ultracut S) and stained by 2% osmium tetroxide solution, which selectively stained the PAESO blocks, prior to imaging.

## **Results**

PS-PAESO block copolymers were synthesized according to Scheme 1. PS macromonomers were polymerized in bulk due to the low reactivity of styrene in RAFT polymerization.

Subsequently, the chain extension was conducted by copolymerizing PS macromonomers with AESO monomers. The final product was washed with methanol followed by cyclohexane, a  $\theta$ -solvent for selectively dissolving polystyrene, <sup>46</sup> to separate out unreacted AESO monomers and PS macromonomers. The properties of PS macromonomers and PS-PAESO block copolymers are summarized in Table 1 and 2. Moreover, the normalized refractive index (RI) traces of each PS-PAESO block copolymer and the corresponding PS macromonomer are provided in Figure S1. In the following we discuss the architecture of PS-PAESO block copolymers followed by their self-assembly behavior and thermal stability properties.

To characterize the architecture of PS-PAESO block copolymers,  $^{1}$ H-NMR spectra, as exemplified in Figure 1, are used to calculate the composition, the degree of polymerization (DP), and the branching extent of PAESO blocks. The composition as determined by the ratio of styrene and the terminal methyl groups on the AESO side chains is summarized in Table 2. The subsequent DP of the overall and individual blocks can be derived based on the composition and the molecular weight of PS assisted by GPC as following:

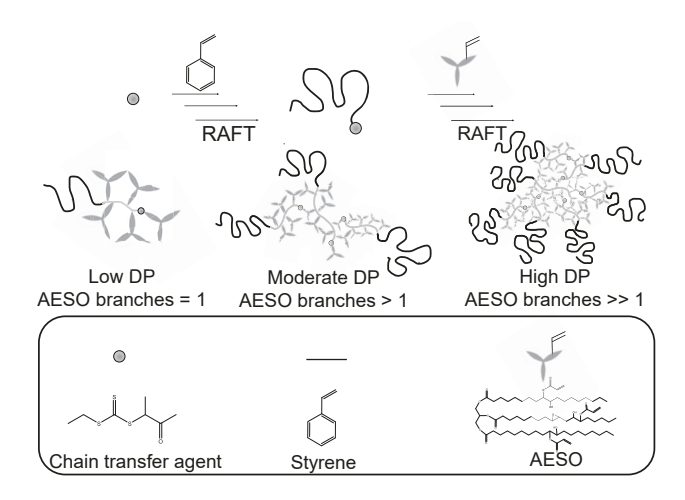
$$DP_{PS} = M_{w,PS}/w_S \tag{1}$$

$$DP_{PAESO} = DP_{PS} * \frac{1 - m_{PS}}{m_{PS}} \tag{2}$$

where  $DP_{PS}$  is DP of polystyrene block,  $w_S = 104.15 \ Da$  is the molecular weight of a styrene repeating unit,  $DP_{PAESO}$  is the DP of PAESO block,  $m_{PS}$  is the molar ratio of styrene block based on <sup>1</sup>H-NMR spectra. Results are summarized in Table 3.

The quantification of the branched architecture in PAESO requires careful consideration. In star polymers, the appropriate descriptor is simply the number of arms, which follows directly from the functionality of the linking agent. However, while AESO monomers are multi-functional, only a small fraction of this excess functionality is con-

sumed. Once integrated into a parent chain, most of remaining pendent vinyl groups may survive the entirety of the polymerization process unscathed; those that participate in subsequent propagation reactions become branch points. Branching events will primarily be intermolecular attacks by PS or PS-PAESO macroradicals or intramolecular loop-forming reactions. Intermolecular branching leads to a star-like accumulation of PS blocks throughout the PS-PAESO architecture. The placement of branch points will be stochastically distributed throughout the PS-PAESO graph, as will be the composition and molecular weight of each arm in PS-PAESO. Thus unlike precisely constructed star polymers where the number of branches and characteristics of each branch are essentially uniform, the architecture of hyperbranched PS-PAESO must be described through the use of average properties. We define the branch number B = n - p, where n is the number-average functionality of the branching monomer mixture (AESO, n = 2.6); and p is number-average of vinyl groups remaining in the polymer. B is unity for a strictly linear polymer and approaches the functionality of the branching monomer when all excess functionality is converted to branch points. B thus directly reflects the branch point density although it cannot differentiate between the intermolecular and intramolecular crosslinking. Scheme 1 illustrates the ideal block copolymer architecture of PS-PAESO with different branch numbers assuming no intramolecular crosslinking is involved. The number of PS arms in the block copolymer grows dramatically as B increases. The value of *B* is summarized in Table 3.



Scheme 1: RAFT polymerization for PS-PAESO of the different branch number and degree of polymerization.

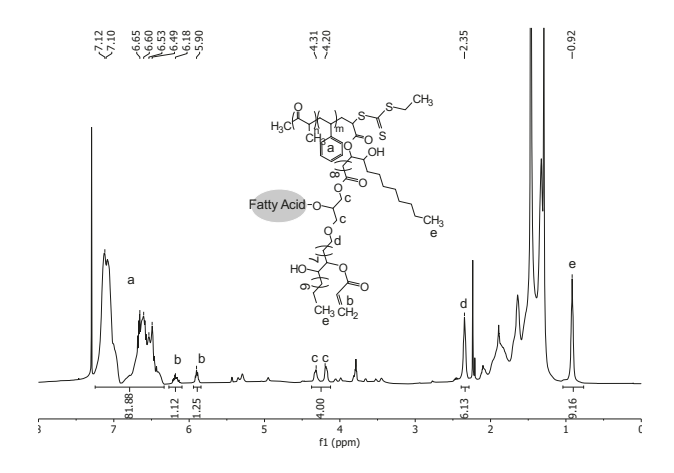


Figure 1: The <sup>1</sup>H NMR spectra of a representative PS-PAESO, which contains an average of 1.19 residual pendent vinyl groups according to peak b integral.

Table 1: Characteristic of PS macromonomer

Entry	$M_w$ a/Da	Đ	$T_{g,PS}$ / $^{o}C$
H1	114 166	1.16	112.80
H2	90 629	1.18	111.90
H3	40 351	1.10	107.78
<b>H4</b>	29 045	1.14	106.75
H5	17 342	1.09	103.43
H6	13 686	1.06	102.96
H7	12 529	1.08	100.46

 $<sup>^</sup>a$ Weight-average molecular weight ( $M_w$ ) is obtained from triple detection.

Table 2: Characteristics of PS-PAESO block copolymers

Entry	Entry PS precursor $M_w / \mathrm{Da}^a$	$M_w / \mathrm{Da}^a$	Э	$f_{PS}^{b/o/o}$	$T_{g,PS}$ / $^{o}C^{\mathrm{c}}$ $T_{g,PAESO}$ / $^{o}C^{\mathrm{c}}$	$T_{g,PAESO}$	$W_{sol}$ /% $Q_{M}^{ m e}$	$Q_M^{ m e}$	d /nm <sup>f</sup>
Symmetric	tric								
BS1	H2	117 653	1.50	52	102.78	-9.89	27.41	5.70	110
BS2	H4	36 129	1.58	52	91.41	-21.24	36.31	2.86	48
BS3	BS3 H5	39 120	1.54	46	79.81	-20.29	13.68	2.77	23
PAESO-	rich asymmet	ric							
BAA1	H1	303 745	1.57	33	108.30	4.27	31.70	4.75	155
BAA2	9H	31 714	1.21	22	ı	-1.92	3.69	3.45	23
BAA3	H7	18 982	1.76	35	I	-19.61	26.34	2.99	I
PS-rich	S-rich asymmetric								
<b>BAS1</b>	, H3	62 441	1.36	63	97.21	-7.05	98.30	ı	43
BAS2	H5	26 526	1.21	29	78.71	-21.31	37.45	7.58	22
BAS3	H7	15 815	1.48	65	69.70	-17.93	38.05	3.45	ı

 $^{a}$ To account for the non-linear architecture of PS-PAESO, weight-average molecular weight  $(M_{w})$  is reported from triple detection.

<sup>b</sup>Volume fraction of PS ( $f_{PS}$ ) is based on <sup>1</sup>H NMR results. The density of styrene and AESO used in the calculation is 0.91 and 1.06  $g/cm^3$ , respectively. <sup>c</sup>Based on DSC curves. The PS block is too small for DSC to capture  $T_{g,PS}$  in **BAA2** and **BAA3**.

<sup>f</sup>Based on SAXS spectra. The domain spacing (d) is calculated from the  $q^*$  of primary peak such that  $d = 2\pi/q^*$ .

<sup>&</sup>lt;sup>e</sup>Weight-based swelling ratio ( $Q_M$ ) after annealing is defined as he weight of the blotted dry gel part over the difference between the original sample and the sol part. Most **BAS1** remained in the sol form thus its  $Q_M$  is omitted.  $^d$ Weight-based sol fraction ( $W_{sol}$ ) after annealing is defined as the fraction of the sol to the original sample.

Table 3: Details of block copolymer architecture calculated from GPC and <sup>1</sup>H NMR results

BS1       1.30       870         BS2       1.03       279         BS3       0.95       167         BAA1       2.23       1 096	76 25 18	946 304					
	25 18	304		6.7	92	181 330	0.65
	18		816	2.2	92	59 320	0.61
` '		185	538	1.6	06	39 188	1.00
	228	1 324	2 368	20.3	83	388 132	0.78
	46	177	556	4.0	74	68 401	0.46
<b>BAA3</b> 1.16 120	23	143	542	2.0	84	39 866	0.48
	23	410	938	2.0	94	67 441	0.93
	8	175	382	0.7	95	27 280	0.97
<b>BAS3</b> 0.93 120	9	126	275	0.5	96	19 315	0.82

 $^a$ Branch number B calculated based on  $^1$ H NMR results.

 $^{b}$ Overall degree of polymerization  $DP = DP_{PS} + DP_{PAESO}$   $^{c}$ Number of statistical segment N considers the volume difference between styrene and AESO repeating units.  $N = DP_{PS} * v_{PS}/v_{ref} + DP_{PAESO} * v_{PAESO}/v_{ref}$ , where  $v_{PS} = 107 \ cm^3/mol$ ,  $v_{PAESO} = 1118 \ cm^3/mol$ , and  $v_{ref} = 71.1 \ cm^3/mol^{47}$  and  $v_{ref} = 71.1 \ cm^3/mol^{47}$  doubtour length  $\ell = DP_{PAESO} * 0.154 * \cos{(109.5^{o}/2)}$  where  $0.154 \ nm$  and  $109.5^{o}$  are the length and angle of  $sp^3$  C-C

bond.

The self-assembly of PS-PAESO block copolymers was investigated using SAXS after thermal annealing. To accelerate the annealing process at moderate temperature, 20 wt% of Eastman 168 (P), a bis(2-ethylhexyl) terephthalate-based plasticizer, was blended with the block copolymers. With its high boiling point and low vapor pressure, Eastman 168 is widely used in commercial purposes. The spectra of neat and plasticized (denoted with suffix P) block copolymers are shown in Figure 2. Most of PS-PAESO entries reveal broad signals from the primary peak except **BAA3** and **BAS3** which do not phase separate given the smaller molecular weights. However, we do not observe the clear signal of the higher-order peaks indicative of long-range order. The broad primary peak along with the absence of higher ordered peaks implies that PS-PAESO block copolymers are dynamically frustrated, *i.e.*, they are unable to reach equilibrium. A report by Balsara *et al.* revealed that the higher ordered peaks can be suppressed and even be absent in highly crosslinked block copolymer systems.<sup>25</sup> Though lacking a crystallographically-defined morphology, the domain spacing (d) of PS-PAESO microstructures can still be derived from the equation  $d=2\pi/q^*$  based on the primary peak, which is summarized in Table 2. It is apparent that d is highly related to the overall DP and the branch number. Entries with a higher DP and branch number generally have a larger d.

Figure 3 displays representative TEM micrographs; PAESO domains are selectively stained dark with OsO<sub>4</sub> through the residual vinyl groups. <sup>48</sup> Further evidence of kinetically-trapped self-assembly can be observed in Figure 3c,e while Figure 3a, g remain more disordered-like structures. Aggressive thermal annealing is precluded in PS-PAESO due to the slow dynamics of morphology coarsening with respect to the speed of PAESO crosslinking. Our previous study on the chain relaxation of hyperbranched PAESO homopolymers has pointed out the relaxation time of PAESO drastically prolongs with increasing branching and molecular weight. <sup>37</sup> Nevertheless, the softened plasticized blends (Figure 3b,d,f,h) reveals improved structures with similar domain spacing but comparatively more developed long-range order though dynamic frustration still exists. Micro-

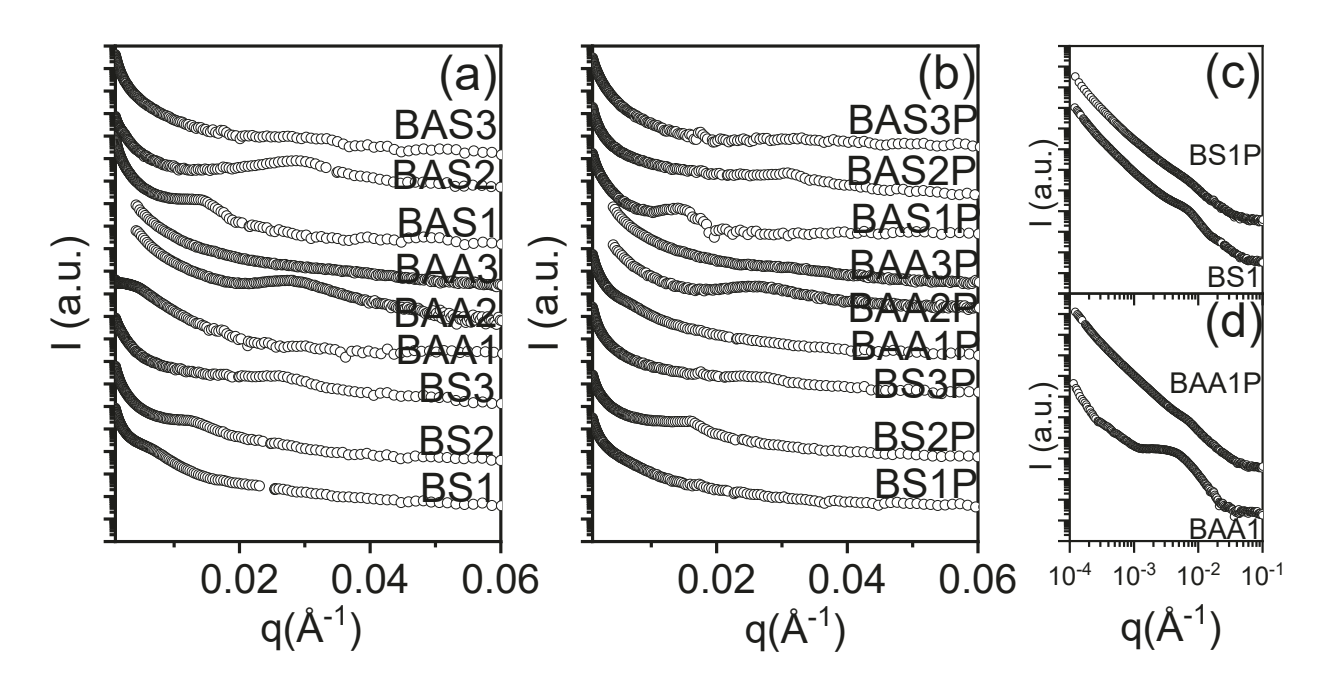


Figure 2: SAXS spectra of (a) neat and (b) plasticized PS-PAESO block copolymers at room temperature. The enlarged spectra for (c) **BS1/BS1P** and (d) **BAA1/BAA1P** in loglog scale.

graphs of **BS3P**, **BAA1P** and **BAS2P** suggest lamellar morphologies while **BAS1P** appears to be hexagonally packed PAESO cylinders in a PS matrix. Both TEM micrographs and SAXS spectra show that the incorporation of plasticizer does not significantly affect the domain spacing. Despite the long-range order of microstructures being significantly improved according to TEM micrographs, higher-order peaks remain undetectable in SAXS spectra. The scattering length density of Eastman 168 is  $9.01 \times 10^{-6} \text{Å}^{-2}$ , which is intermediate to that of PS  $(9.57 \times 10^{-6} \text{Å}^{-2})$  and PAESO  $(8.34 \times 10^{-6} \text{Å}^{-2})$ . Hence when blending Eastman 168 with PS-PAESO block copolymers, the decrease of scattering contrast between blocks may have resulted in the lack of obvious higher ordered peaks.

The time and energy required for block copolymers to reach the equilibrium state are highly related to polymer chain mobility, which is implied by the glass transition temperature  $(T_g)$ .  $T_g$ s of the block copolymers and PS macromonomers provide the information of polymer chain mobility as listed in Table 1 and 2. The  $T_g$  of PS blocks  $(T_{g,PS})$  in **BAA2** and **BAA3** is not detectable through DSC due to the large PAESO content.  $T_{g,PS}$  in

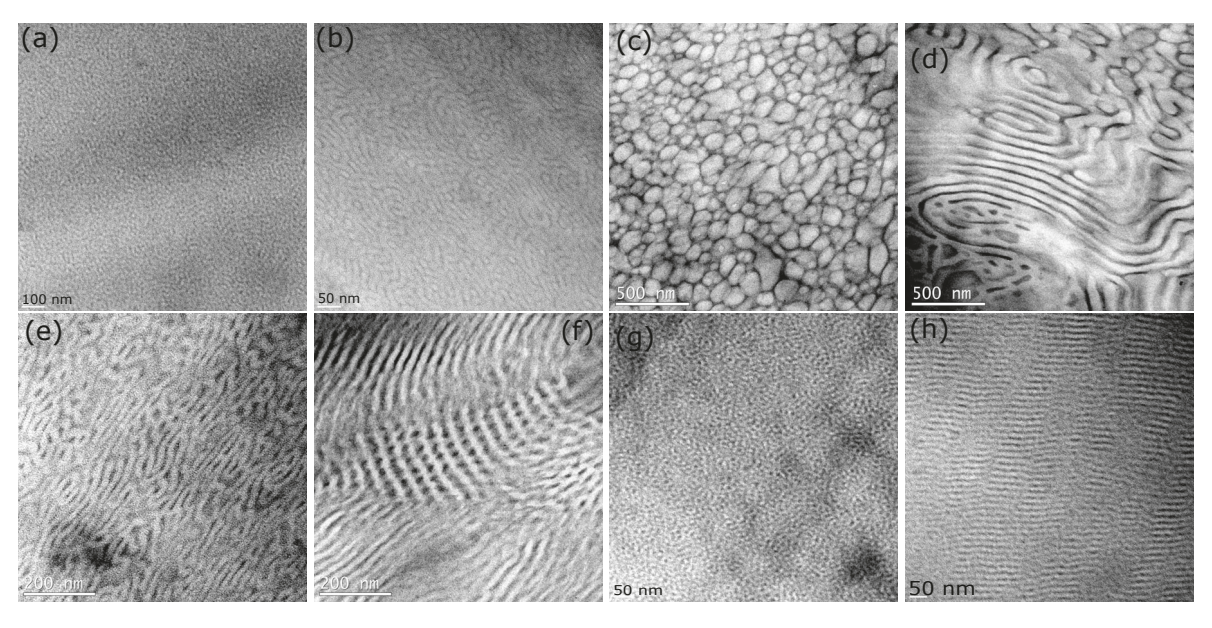


Figure 3: TEM micrographs of (a)BS3, (b)BS3P, (c)BAA1, (d)BAA1P, (e)BAS1, (f)BAS1P, (g)BAS2, and (f)BAS2P. Black and white domains are PAESO and PS blocks, respectively.

the block copolymers generally drops compared to its macromonomer precursor, which becomes more apparent as the molecular weight of polymers decreases. Since the segregation strength is weakened by the decrease of the molecular weight, PS blocks are softened by mixing with PAESO. For example, in **BAS3**, which does not show phase separation in SAXS spectra,  $T_{g,PS}$  is about 30 °C lower than its PS macromonomer counterpart.  $T_{g,PAESO}$ s lie between -21 and 4 °C and are affected by the molecular weight and the extent of branching of PAESO blocks. Entries with higher molecular weight and higher branch numbers show higher  $T_{g,PAESO}$  such as **BS2** and **BAA1**. As the mobility of polymer chains is limited by the increased extent of branching in PAESO blocks,  $T_{g,PAESO}$  increases, as seen in Table 2. Moreover, the increase of polymer chain mobility when blending with the plasticizer is also revealed by  $T_g$ s. Figure S3 shows DSC curves of **BAA1** and **BAA1P** pair.  $T_{g,PS}$  drops  $\sim 50$  °C while  $T_{g,PAESO}$  drops below the testing range after plasticizing. This result suggests that Eastman 168 effectively plasticizes both PS and PAESO blocks without strong incorporation preference.

Dynamic shear rheology was used to assess the response of PS-PAESO to heating, particularly in regard to the onset of crosslinking which interferes with thermal equilibration.

Figure 4a shows the isochronal curves of **BAA1** and **BAA1P**. Compared to **BAA1**, the storage modulus curve G'(T) of **BAA1P** is shifted by about 50 °C in agreement with DSC in Figure S2. In the absence of curing reactions, polymers are softened by applying heat until reaching the terminal relaxation regime. Conversely, in PS-PAESO system, PAESO blocks cure during heating. In **BAA1** and **BAA1P** this process becomes rapid near 180 °C where G'(T) passes through a minimum and increases with further heating. The onset of curing occurs at significantly lower temperature. In Figure 4(a), the initial heating of **BAA1** is indicated by the light gray curve. At 190 °C, the sample is then cooled to 60 °C (gray). Between 190 and 150 °C, G'(T) fails to retrace the original curve, with a 50% increase in the G' value that persists as cooling continues to 60 °C. During the final heating cycle (black), G'(T) retraces the cooling curve until about 150 °C where the modulus again begins to increase.

The curing process of PS-PAESO block copolymers is not governed only by radical propagation through pendent vinyl groups of PAESO. To exclude the effect of radicals propagating in curing, the pendent vinyl groups are selectively hydrogenated by reacting them with tosyl hydrazide. The selective hydrogenation saturates on the pendent vinyl groups as shown by the  $^1$ H NMR spectra in Figure S4. The vinyl group signals at  $\delta$  5.86 and 6.13 in **BAS1** vanish in hydrogenated **BAS1H**. Isochronal temperature ramps of preannealed **BAS1** and **BAS1H** are compared in Figure 4(b). Surprisingly, **BAS1H** shows no evidence of softening at temperatures higher than 180  $^{\circ}C$ , which indicates PS-PAESO is considerably cured through another crosslinking mechanism. The onset of curing in PS-PAESO block copolymers is further explained in the discussion.

Another straightforward evidence of curing is provided by the sol fraction and swelling ratio of the pre-annealed samples. Summarized in Table 2, except **BAS1** remains mostly in sol, the rest of samples show different level of gelation and swelling. Yet the most ungelled **BAS1** reveals the incline of G' in Figure 4(b). Therefore, in other samples the interference of thermal equilibration owing to crosslinking can be expected to be even more

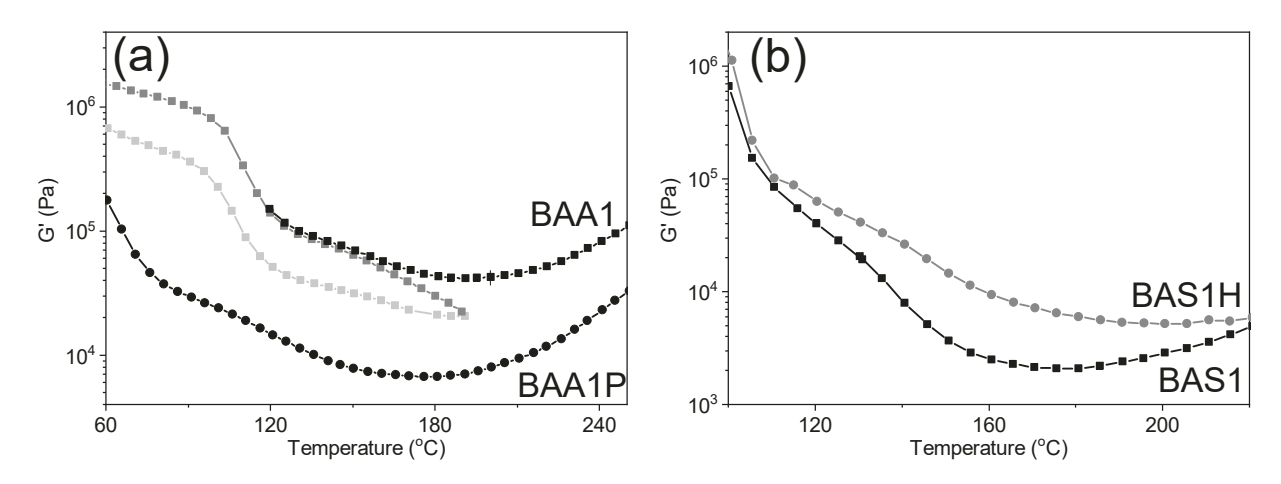


Figure 4: (a) Isochronal temperature ramp of **BAA1** ( $\blacksquare$ ) and **BAA1P** ( $\bullet$ ). The heating history of **BAA1** is revealed by different colors. Lines of light gray, gray, and black are 1<sup>st</sup> heating, 1<sup>st</sup> cooling and 2<sup>nd</sup> heating, respectively; (b) Isochronal test of **BAS1** ( $\blacksquare$ ) and **BAS1H**( $\bullet$ ) during heating cycle.

severe.

The dynamics of PS-PAESO are further investigated through the construction of master curves from isothermal frequency sweeps. Figure 5 displays the master curve of H1, BAA1, and BAA1P. The frequency sweep test was performed on BAA1 from 40-200 °C and BAA1P from 40-230 °C. The fact that the storage modulus G' is always larger than the loss modulus G'' in both BAA1 and BAA1P implies these pre-annealed materials crosslinked during the thermal annealing process before testing. The TTS failure presented at 1-100 rad/s of BAA1 and  $10^4 - 10^5$  rad/s of BAA1P is due to the transition of glassy to rubbery state of PS blocks. Compared to H1 which shows an entanglement plateau and reaches the terminal regime, BAA1 and BAA1P display the second plateau, which indicates another relaxation resistance in place, without the evidence of full relaxation in the testing frame. The different plateaus can be identified by the minimum of the loss factor  $\tan \delta$ , which is defined as G'' over G', in Figure 5(b).

Studies have shown that the extra plateau in the low frequency regime reveals the information of microstructures and phase transitions. <sup>49,50</sup> Hence the second plateau in the low frequency regime  $(10^{-3} - 10^{-5} \text{ rad/s})$  may result from either the microstructure

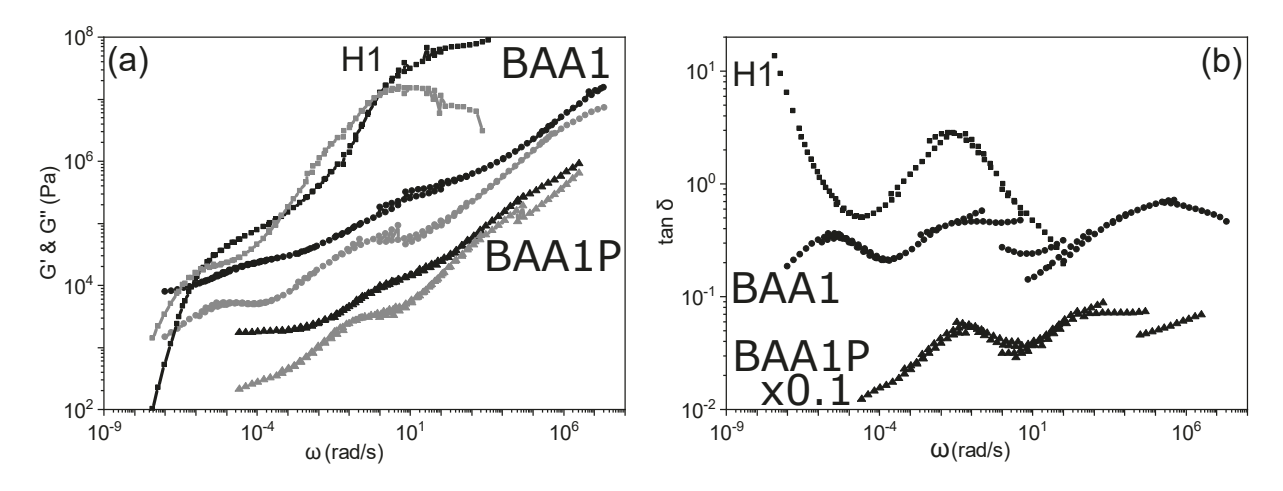
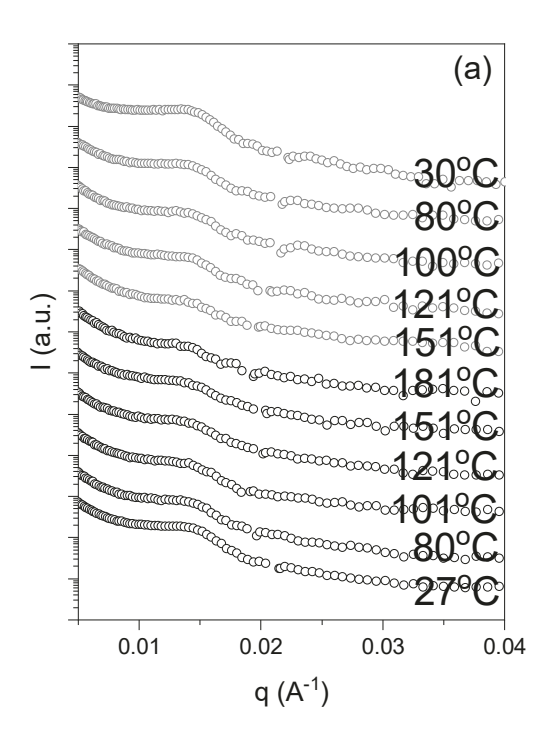


Figure 5: (a) Master curve and (b) the corresponding  $tan\delta$  of **H1**, **BAA1**, and **BAA1P** at the reference temperature of 100 °C. G' and G'' are black and gray, respectively.

of block copolymers or the cured network. To reach this low frequency regime experimentally, the frequency sweep test has to be conducted above  $180\,^{\circ}C$  which corresponds to the onset of G' incline in Figure 4. Therefore, the second plateau is possibly caused by the covalently bonded network structure rather than the physical constraints resulting from block copolymer microstructures. The evidence suggests that block copolymers may not be capable of reaching the equilibrium state due to the pinning effect resulting from PAESO crosslinking.

Additional insights on the response of PS-PAESO to heating can be studied in temperature-dependent SAXS experiments. Figure 6(a) shows I(q) of pre-annealed **BAS1** during a heating and cooling cycle. The SAXS spectra of plasticized **BAS1P** is shown in Figure S3. The maximum temperature, 181  $^{\circ}C$ , was determined based on the isochronal test results so that **BAS1** is cooled before fully cured. The intensity of the primary peak gradually decreases with increasing temperature and the behavior is reversible during cooling. Figure 6(b) shows the intensity change in temperature of **BAS1** and **BAS1P**. **BAS1P** has a similar intensity change behavior as **BAS1**. The decrease of the primary peak indicates that the system becomes more homogeneous at elevated temperature, which is a sign of an upper critical ordering temperature system. As mentioned before, since PS-PAESO cures during

thermal annealing and does not have obvious higher ordered peaks in SAXS spectra, our current data sets do not allow the precise evaluation of the order-disorder transition temperature. However, it would seem that both **BAS1** and **BAS1P** undergo a phase transition between 150 and  $180\,^{\circ}C$ .



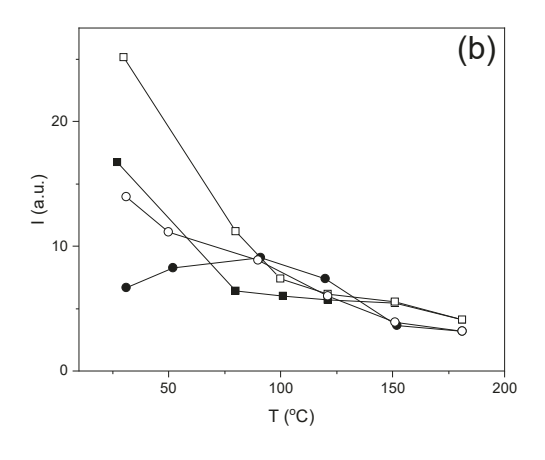


Figure 6: (a) SAXS spectra of **BAS1** during heating( $\circ$ ) and cooling ( $\circ$ ) cycle. (b) The intensity of the primary peak of **BAS1** heating ( $\blacksquare$ ), **BAS1** cooling ( $\square$ ), **BAS1P** heating ( $\bullet$ ), and **BAS1P** cooling ( $\circ$ ).

#### Discussion

The multi-functional characteristic of AESO contributes to different possible architectures for PS-PAESO block copolymers. AESO monomers branch during the polymerization and result in the star-like and star-brush-like architectures of PS-PAESO. Unlike single-cored star polymers which have well-defined polymer arms, the arms in PS-PAESO block copolymers are hard to define due to the stochastic branching nature of PAESO. The determination of the number of PS arms  $(n_{PS})$  in PS-PAESO block copolymers relies on the accuracy of molecular weight along with the block molar ratio. Theoretically, the molecular weight increases dramatically as polymer branches out. Assuming this deviation could be used to calculate  $n_{PS}$ , we obtain

$$MW_{calc} = M_{w,PS} + DP_{PAESO} * w_{AESO}$$
(3)

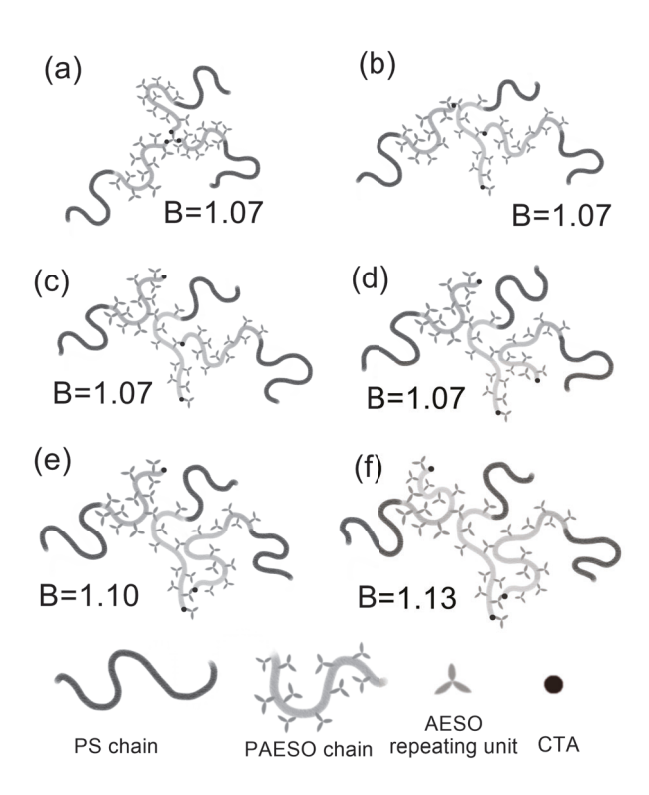
$$n_{PS} = \frac{MW_{exp}}{MW_{calc}} \tag{4}$$

where  $MW_{calc}$  is the calculated molecular weight,  $w_{AESO}=1200\ Da$  is the molecular weight of an AESO repeating unit, and  $MW_{exp}$  is the experimental molecular weight obtained from GPC. The values of  $MW_{calc}$  and  $n_{PS}$  are summarized in Table 3, which are all less than unity. These results suggest that the experimental molecular weight is generally smaller. Experimentally, the fractionation by GPC columns relies on the hydrodynamic radius of polymers. Differed from linear polymers, at a given hydrodynamic radius there are multiple possible chain conformations for non-linear polymers. Hence, the monotonic relationship of the molecular weight and the hydrodynamic radius is broken. Moreover, it is reported that GPC elution becomes abnormal when the degree of branching increases. The retardation of highly branched polymers in columns leads to negatively-deviated molecular weight even when using the triple detection technique. This effect may explain the negatively deviated experimental molecular weight of PS-PAESO block

copolymers compared to the calculated results. This deviation becomes more severe as the molar ratio of PAESO block increases which also suggests the architecture of PAESO block affects the block copolymer behavior in solution. The deviation of the experimental molecular weight impedes the accurate evaluation of  $n_{PS}$  and prompts us to find another way, the branch number, in describing the architecture of PS-PAESO block copolymers.

Scheme 2 demonstrates the complexity of PS-PAESO block copolymer architectures and the utility of the branch number in describing their architectures. In Scheme 2 three PS-PAESO sub chains are considered with the exact same length of PS chains and equal number (10) of AESO repeating units. In this way, the block copolymer will have the same composition and molecular weight based on instrumentation. Since the average functionality of AESO is 2.6 and there are 30 AESO repeating units involved, the initial unreacted vinyl group count is 78 (2.6  $\times$  30). After the reaction, 46 pendent vinyl groups are left in Scheme 2(a)-(d), while 45 and 44 are left in (e) and (f), respectively. In Scheme 2 the branch numbers are thus (78 - 46)/30 = 1.07 for (a)-(d), 1.10 for (e), and 1.13 for (f). The positions of branch points vary since AESO randomly branches during polymerization. Though the overall composition, molecular weight, and branch number are the same for (a)-(d) in Scheme 2, the number of arms and the composition on each arm are considerably different. For example, Scheme 2(a) has three identical PS-PAESO arms and a single branch point, while (b) has three arms with PS chains and one arm of PAESO chain only. PAESO arms can grow longer if radicals continuously propagate after branching. Scheme 2 (e) and (f) demonstrate the more complicated cases when intramolecular crosslinking takes place. As PAESO loops are formed by the intramolecular crosslinking, the number of arms is even harder to define. Therefore, the expression of the branch number gives a better insight of PS-PAESO architectures than the number of arms.

The consideration of PS-PAESO architectures cannot leave the unique AESO conformation without. As DP increases, the backbone of PAESO blocks elongates which changes the conformational behavior of PS-PAESO from star-like to star-brush-like. This



Scheme 2: An illustration of the different branched architectures of PS-PAESO block copolymer with the same composition and sub chain length. The figure shows three sub chains and each one has 10 AESO repeating units. The branch number *B* is the average number of vinyl groups reacted in AESO monomers, which directly reflects the branch density.

depends on the relative length of the brush and the backbone of PAESO blocks, which can be evaluated by the contour length. The contour length of the furthest AESO pendent group terminus from the acrylic backbone is ca.  $\ell_{AESO}=2.93~nm$  as illustrated in Figure S6; this value is an important characteristic of PS-PAESO architecture. Summarized in Table 3, the contour length of PAESO backbones in the block copolymers is calculated from  $\ell=DP_{PAESO}*0.154*\cos(109.5^o/2)$  where 0.154 nm and  $109.5^o$  are the length and angle of  $sp^3$  C-C bond. If the backbone contour length is less than 3~nm, the architecture of PS-PAESO resembles star block copolymers; whereas the others shall be described as star-brush block copolymers.

The multi-functional characteristic of AESO not only results in the star-like and starbush-like architectures of PS-PAESO but also contributes to curing during the thermal

annealing process. The pendent vinyl groups of AESO left from the polymerization further cure through radical propagation. However, based on our isochronal test result in Figure 4(b) we found out that radical propagation may not be the only cause of curing since curing still takes place after all pendent vinyl groups are hydrogenated. We thus suspect that the transesterification within PAESO also contributes to the curing process. Soybean oil, the fatty acid ester, has three active sites for transesterification. The number of active sites further increases as acrylic groups conjugate onto soybean oil via ester links. The transesterification reaction is a reversible reaction that takes places simply by mixing reactants and can be accelerated with the assistance of catalysts.<sup>52</sup> An exchange of a subtle number of ester groups is enough to alter the polymer architecture and leads to curing. The curing process prevents PS chains from escaping PAESO block and thus leaves the morphology in the non-equilibrium state, which is evidenced by the drop of  $T_{q,PS}$  in PS-PAESO compared to its PS macromonomer precursor. Sakurai et al. mentioned that the annealing time required for crosslinked block copolymers to show higher ordered peaks in SAXS spectra is much longer even at low extent of crosslinking.<sup>23</sup> Their pre-annealed samples show poor long range order in TEM micrographs, which indicates that crosslinked block copolymers are harder to reach the equilibrium state. Balsara et al. also observed a gradual loss of long-range order in block copolymer self-assembly with increasing crosslink content in both SAXS spectra and TEM micrographs when PI is selectively crosslinked in PS-PI block copolymers. <sup>25,26</sup> Our SAXS and TEM results are consistent with previous studies. That is, the crosslinking-involved self-assembly of block copolymers makes it hard to preserve the morphology with a good long-range order.

One critical parameter in block copolymer self assembly behavior is the system's segregation strength ( $\chi N$ ), where  $\chi$  and N are the interaction parameter and number of statistical segments, respectively. The self assembly of symmetric linear diblock copolymers takes place when  $\chi N > \chi N_{ODT} = 10.5$  as first shown using the random-phase approximation. For star block copolymers,  $(\chi N_{arm})_{ODT}$  decreases with increasing number of

arms calculated by mean-field theory. 15,16 This behavior is supported experimentally in the well-defined PS-PI star block copolymer system. <sup>20</sup> Olmsted and Milner considered  $A_nB_m$  miktoarm star polymers with the strong segregation theory and showed that the entropic stiffness of the B domain scales as  $\frac{m^2}{n^2}$ ; 17,54 this asymmetry expands the stability of strongly curved interfaces favoring the less-branched domain. Grason evaluated SCFT for AB diblock copolymers with a well-defined hyperbranched architecture of up to 6 generations. 55 This work further illustrated the shift in phase boundaries favoring the linear A block, and of particular interest to the present work, indicates  $\chi N_{ODT} \in [11, 13]$ for  $f \in [0.4, 0.7]$  for the most heavily branched model. The stochastic nature of PAESO branching and the dynamic frustration during annealing makes complicates the calculation of a precise value of  $\chi N_{ODT}$  for this system. Moreover, the different structure between styrene and AESO repeating units results in the dramatic specific volume difference when calculating N as listed in Table 3. Nonetheless, the Grason result suggests  $\chi N_{ODT} \in [11, 13]$  is a reasonable first approximation that can be used to estimate the  $\chi$ value for PS-PAESO. Comparing N and Figure 2, we would be able to roughly locate the order-disorder boundary since BAA3 and BAS3 are disordered while BS3, BAA2 and BAS2 display characteristic peaks. The boundary seems slightly skew to PS-rich side as **BAS2** self-assembles at N=382. Based on these observations, we estimate that the  $\chi$ value of PS-PAESO to be in the range 0.019-0.035 depending on the composition. A more precise evaluation of  $\chi$  will require a more detailed description of the PS-PAESO architecture and an accompanying model that properly accounts for dispersity, branch point distribution including looping.

To investigate the influence of polymer architectures on the domain spacing, Figure 7a compares the domain spacing (D) with respect to the branch number (B) for PS-PAESO, or the number of arms (n) for the (PS-PI)<sub>n</sub> star polymers reported by Ijichi  $et\ al.^{20}$  The domain spacing is normalized by the number of statistical segments as  $\frac{D}{N^x}$  to exclude the molecular weight influence on domain spacing; a properly chosen scaling exponent x

will yield a horizontal line. Studies have shown that domain spacing of star block copolymers<sup>56,57</sup> and miktoarm copolymers<sup>58</sup> follow the same scaling as strongly segregated linear block copolymers with  $D \propto N^{2/3}$ . The normalized domain spacing of PS-PAESO  $\frac{D}{N^{0.67}}$ vs. B is shown with gray filled symbols in Figure 7(a); there is clearly an increasing dependence with the value of B. Conversely, the domain spacing of star (PS-PI)<sub>n</sub> is nearly independent of number of arms. This is consistent with simulation and experimental results of star block copolymers which indicate the number of arms does not affect the domain spacing at fixed arm length. 19,20,56-59 The domain scaling of PS-PAESO significantly differs from star block copolymers and miktoarm copolymers. This implies that another architectural feature, the inherently brush-like character of PAESO arising from its bulky aliphatic acid side chains, plays an important role determining the domain size. Figure 7(b) compares the domain spacing of PS-PAESO with the brush block copolymers (BrBCP)s reported by Gu et al.  $^{30}$  against N. The BrBCPs are composed by two different side chains, polystyrene and polylactide, with the same polynorbornene backbones. The molecular weight dependence of *D* in PS-PAESO is similar to that BrBCPs with a rod-like scaling exponent x = 1.05. The slope of PS-PAESO is slightly higher than BrBCPs, which implies that the non-linear brush-like character of PAESO promotes the domain expansion more strongly than linear brushes. The PS-PAESO data sets shown in black in Figure 7(a) with x = 0.95 yields similar behavior to (PS-PI)<sub>n</sub> such that the branch number does not directly impact domain size. This finding implies that the unusual domain expansion of PS-PAESO block copolymers in high N entries, especially in **BS1** (D = 110 nm) and **BAA1** (D = 155 nm), is due to the brush-like character of the PAESO blocks.

The influence of  $\mathcal{D}$  should also be taken into account on domain expansion. Since PS-PAESO was prepared by RAFT polymerization with multi-functional AESO monomers,  $\mathcal{D}$  of the final products ranges from 1.21 to 1.58 for the phase-separated entries. Compared to nearly-monodisperse block copolymers prepared from anionic polymerization, the domain spacing of polydisperse block copolymers is expected to increase. The increase of

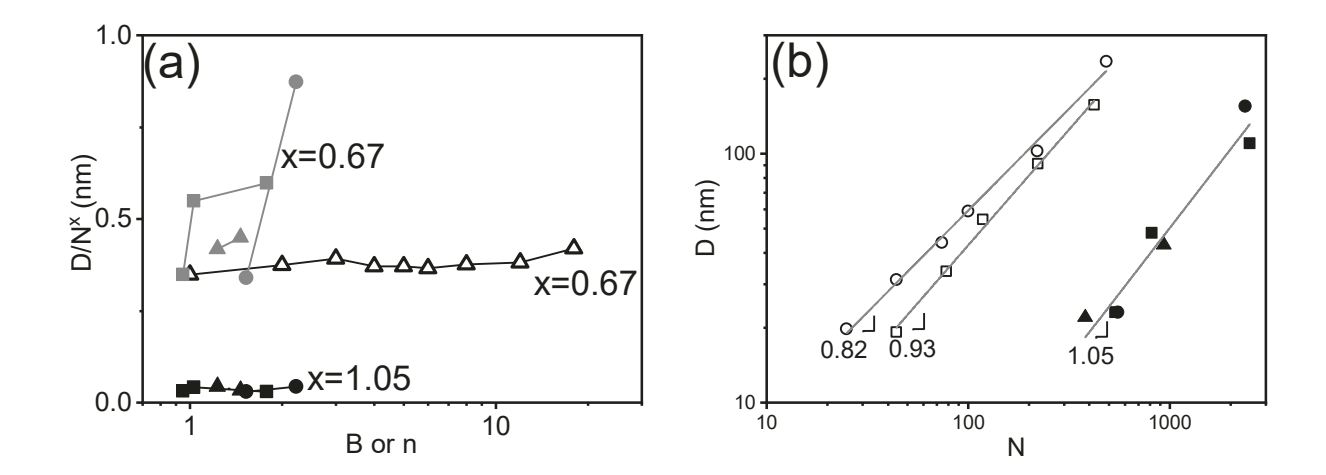


Figure 7: Analysis of the domain-size scaling behavior of PS-PAESO (**BS** series  $\blacksquare$ , **BAS** series  $\blacktriangle$ , and **BAA** series  $\bullet$ ) compared with block copolymer brushes with different brush lengths  $^{30}$  ( $\square$  and  $\circ$ ) and PS-PI stars  $^{20}$  ( $\triangle$ ). (a)  $D/N^x$  vs. B for PS-PAESO or n for star PS-PI from Ijichi  $et\ al.^{20}$  Gray symbols show failure of PS-PAESO to conform to the x=0.67 scaling exponent. (b) Domain spacing vs. the number of statistical segments (N) for PS-PAESO and BrBCPs from Gu  $et\ al.^{30}$  The linear regression of PS-PAESO gives  $D\propto N^{1.05}$  with  $r^2=0.94$ .

domain spacing with increasing  $\mathcal{D}$  is well-documented in linear block copolymer systems. Lynd et~al. reported that the domain spacing expands about 1.5 times more than the monodisperse block copolymer as  $\mathcal{D}$  reaches 2 in poly(ethylene-alt-propylene)-block-poly(DL-lactide) systems. Noro et~al. also revealed that the expansion of domain spacing reaches 1.16 times more than the monodisperse counterpart in polystyrene-b-poly-2-vinylpyridine systems. However, the scaling behavior of PS-PAESO block copolymers revealed in Figure 7(b) indicates the extent of domain expansion is more than the contribution of increasing  $\mathcal{D}$  alone. We thus conclude that the domain expansion of PS-PAESO is a combination effect of  $\mathcal{D}$  and brushes from the unique structure of PAESO.

Figure 8 illustrates the expansion of domain spacing with increasing DP and branch number. When the DP and branch number are small, the PAESO block primary chain is short and AESO side chains act as the "arms" of the star structure. The self-assembly behavior of PS-PAESO is therefore similar to star block copolymers as in Figure 8(a) and (d). As DP increases, which usually accompanied by the increase of the branching number,

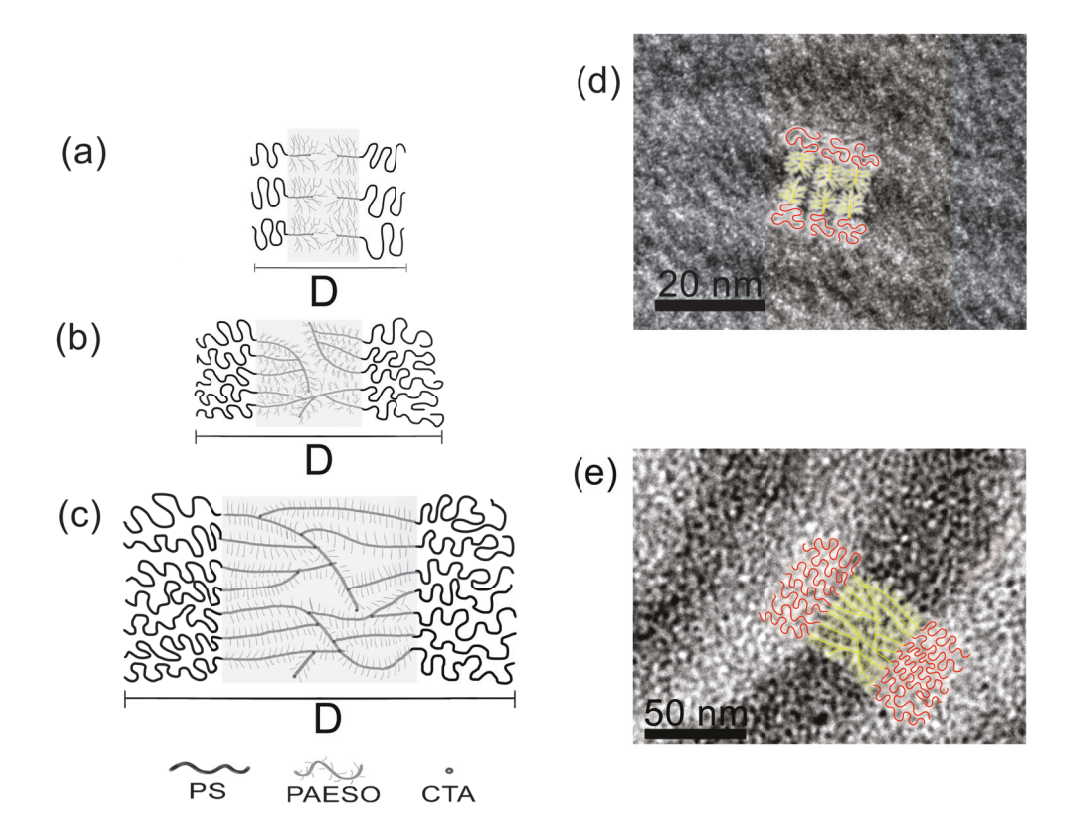


Figure 8: Depiction of domain spacing change with respect to different PS-PAESO architecture. The branch number and the degree of polymerization increases from (a) to (c). The polymer chain packing in (a) and (c) is superimposed on TEM micrographs of **BAS2P** and **BS1P** in (d) and (e), respectively.

the backbone of PAESO blocks grows longer and AESO side chains become the "brushes" as depicted in Figure 8(b), (c), and (e). These brushes impose a conformational constraint on the primary chains which behave more rod-like. The stretching entropy penalty is offset through the packing frustration of the bulky AESO side chains. While these non-linear side chains sufficiently fill the extra space from the expansion, the several-fold number of chain ends compared to linear side chains further increases the systematic entropy. In summary, the domain expansion observed in high DP PS-PAESO block copolymers is mainly susceptible to the star-brush-like architectures with the minor impact of D. This study shows that by utilizing the unique conformation of biobased AESO monomers, non-linear star-brush-like block copolymers with distinctive self-assembly behavior can

be obtained without tedious synthesis steps.

### Conclusion

PS-PAESO block copolymers are derived from the chain extension of polystyrene macromonomers with AESO via RAFT polymerization. The architecture of PS-PAESO varies from star-like to star-brush-like resulting from the *DP* and the multi-functional nature of AESO. Because of the bulky side chain of PAESO, PS-PAESO with a low *DP* resembles star block copolymers as PAESO side chains serve as the star "arms." When *DP* increases, the backbone of PAESO blocks is further developed and PAESO side chains thus become the "brushes." Under this condition, PS-PAESO is better described as a star-brush-like block copolymer, where the star-like character comes from the accumulation of multiple arms during polymerization. Due to the stochastic branching nature of AESO, the architecture of PS-PAESO is described by the branch number to account for the overall extent of branching. A higher branch number means more branch points and a higher number of arms in the star-like architecture.

In addition to branching during polymerization, PAESO blocks further cure during thermal annealing or melt processing as gels present and swell in solvent. Since curing reduces chain mobility, PS-PAESO morphologies will tend to be kinetically trapped with poorly developed long range order; plasticizers improve long-range ordering slightly, but the system remains dynamically limited. To gain further insight into the role of curing on kinetic trapping, the residual vinyl groups in PS-PAESO were selectively hydrogenated. While the rate of curing in hydrogenated PS-PAESO was reduced compared to its precursor, the temperature-driven increase in storage modulus indicated that transesterification was also an important mechanism of PS-PAESO curing.

The domain spacing of PS-PAESO is nearly linear with molecular weight. Similar domain scaling behavior has been reported in bottle-brush block copolymers. The domain

expansion of PS-PAESO can thus be rationalized as: the PAESO side chain brushes interfere the relaxation of its backbone and prevent the backbone from reaching the freely-coil conformation; the entropy penalty of PAESO backbone stretching out is offset by the crowding of AESO non-linear brushes. The degree of branching, as characterized by the branch number *B*, appears to have no direct impact on the domain spacing. This observation is consistent with the invariance of domain spacing to the number of arms in star-block copolymer self-assembly.

Our findings suggest that biobased monomers like vegetable oil derivatives can enable novel block copolymer architectures with distinctive self-assembly behavior through facile synthetic procedures. The ease with which PS-PAESO forms structures with domain spacings greater than  $100\ nm$  offers new strategies for designing biobased polymeric materials with sub-micron features, potentially offering a route to materials with properties useful for optical or filtration applications.

# Acknowledgement

The authors thank the support by United States Department of Agriculture (USDA-NIFA-CAM 2014-38202-22318) and United Soybean Board (USB 1740-362-0710). This research used resources of the Advanced Photon Source, a U.S. Department of Energy (DOE) Office of Science User Facility operated for the DOE Office of Science by Argonne National Laboratory under Contract No. DE-AC02-06CH11357. The authors are grateful to Drs. Jan Ilavsky and Ivan Kuzmenko for their assistance with operating the USAXS instrument on beamline 9-ID. The Xenocs Xeuss 2.0 UHR system was acquired with the support of a Materials Research Instrumentation grant from the National Science Foundation, award No. 1626315.

# **Supporting Information Available**

GPC traces, the calculation of PS arms number, table of number of PS arms and PAESO contour length, SAXS spectra of PS-PAESO/P blends, temperature-dependent SAXS spectra of **BAS1P**, <sup>1</sup>H NMR spectra of **BAS1H**, and the architecture of the AESO repeating unit.

This material is available free of charge via the Internet at http://pubs.acs.org/.

## References

- (1) Bates, F. S.; Fredrickson, G. H. Block copolymers-designer soft materials. *Physics Today* **1999**, 52, 32–38.
- (2) Cochran, E. W.; Garcia-Cervera, C. J.; Fredrickson, G. H. Stability of the gyroid phase in diblock copolymers at strong segregation. *Macromolecules* **2006**, *39*, 2449–2451.
- (3) Leibler, L.; Benoit, H. Theory of correlations in partly labelled homopolymer melts. *Polymer* **1981**, 22, 195–201.
- (4) Lynd, N. A.; Hillmyer, M. A. Influence of polydispersity on the self-assembly of diblock copolymers. *Macromolecules* **2005**, *38*, 8803–8810.
- (5) Noro, A.; Cho, D.; Takano, A.; Matsushita, Y. Effect of molecular weight distribution on microphase-separated structures from block copolymers. *Macromolecules* **2005**, *38*, 4371–4376.
- (6) Burger, C.; Ruland, W.; Semenov, A. N. Polydispersity Effects on the Microphase-Separation Transition in Block Copolymers. *Macromolecules* **1990**, 23, 3339–3346.
- (7) Fredrickson, G. H.; Sides, S. W. Theory of polydisperse inhomogeneous polymers. *Macromolecules* **2003**, *36*, 5415–5423.

- (8) Sides, S. W.; Fredrickson, G. H. Continuous polydispersity in a self-consistent field theory for diblock copolymers. *Journal of Chemical Physics* **2004**, 121, 4974–4986.
- (9) Cooke, D. M.; Shi, A. C. Effects of polydispersity on phase behavior of diblock copolymers. *Macromolecules* **2006**, *39*, 6661–6671.
- (10) Matsen, M. W. Effect of large degrees of polydispersity on strongly segregated block copolymers. *European Physical Journal E* **2006**, *21*, 199–207.
- (11) Lynd, N. A.; Meuler, A. J.; Hillmyer, M. A. Polydispersity and block copolymer self-assembly. *Progress in Polymer Science (Oxford)* **2008**, *33*, 875–893.
- (12) Lynd, N. A.; Hillmyer, M. A. Effects of Polydispersity on the OrderDisorder Transition in Block Copolymer Melts. *Macromolecules* **2007**, *40*, 8050–8055.
- (13) Price, C.; Watson, A. G.; Chow, M. T. An investigation of the effect of chain geometry on the two-phase morphology of polystyrene/polyisoprene block copolymers. *Polymer* **1972**, *13*, 333–336.
- (14) Park, J.; Jang, S.; Kim, J. K. Morphology and microphase separation of star copolymers. *Journal of Polymer Science, Part B: Polymer Physics* **2015**, 53, 1–21.
- (15) de la Cruz, M. O.; Sanchez, I. C. Theory of Microphase Separation in Graft and Star Copolymers. *Macromolecules* **1986**, *19*, 2501–2508.
- (16) Matsen, M. W.; Schick, M. Microphase Separation in Starblock Copolymer Melts. *Macromolecules* **1994**, 27, 6761–6767.
- (17) Milner, S. T. Chain Architecture and Asymmetry in Copolymer Microphases. *Macro-molecules* **1994**, 27, 2333–2335.
- (18) Kinning, D. J.; Thomas, E. L.; Alward, D. B.; Fetters, L. J.; Handlin, D. L. Sharpness of the functionality-induced structural transition in poly(styrene-isoprene) star block copolymers. *Macromolecules* **1986**, *19*, 1288–1290.

- (19) Alward, D. B.; Kinning, D. J.; Thomas, E. L.; Fetters, L. J. Effect of Arm Number and Arm Molecular Weight on the Solid-State Morphology of Poly(styrene-isoprene) Star Block Copolymers. *Macromolecules* **1986**, *19*, 215–224.
- (20) Ijichi, Y.; Hashimoto, T.; Fetters, L. J. Order—Disorder Transition of Star Block Copolymers. 2. Effect of Arm Number. *Macromolecules* **1989**, 22, 2817–2824.
- (21) Koh, M. L.; Konkolewicz, D.; Perrier, S. S. A simple route to functional highly branched structures: RAFT homopolymerization of divinylbenzene. *Macromolecules* **2011**, *44*, 2715–2724.
- (22) Walther, A.; Goldmann, A. S.; Yelamanchili, R. S.; Drechsler, M.; Schmalz, H.; Eisenberg, A.; Müller, A. H. E. Multiple Morphologies, Phase Transitions, and Cross-Linking of Crew-Cut Aggregates of Polybutadiene-block-poly(2-vinylpyridine) Diblock Copolymers. *Macromolecules* **2008**, *41*, 3254–3260.
- (23) Sakurai, S.; Iwane, K.; Nomura, S. Morphology of Poly(styrene-block-butadiene-block-styrene) Triblock Copolymers Cross-Linked in the Disordered State. *Macro-molecules* **1993**, *26*, 5479–5486.
- (24) Hahn, H.; Eitouni, H. B.; Balsara, N. P.; Pople, J. A. Responsive Solids from Cross-Linked Block Copolymers. *Physical Review Letters* **2003**, *90*, 4.
- (25) Hahn, H.; Chakraborty, A. K.; Das, J.; Pople, J. A.; Balsara, N. P. Order-disorder transitions in cross-linked block copolymer solids. *Macromolecules* **2005**, *38*, 1277–1285.
- (26) Gomez, E. D.; Das, J.; Chakraborty, A. K.; Pople, J. A.; Balsara, N. P. Effect of cross-linking on the structure and thermodynamics of lamellar block copolymers. *Macro-molecules* **2006**, *39*, 4848–4859.
- (27) Runge, M. B.; Bowden, N. B. Synthesis of high molecular weight comb block copoly-

- mers and their assembly into ordered morphologies in the solid state. *Journal of the American Chemical Society* **2007**, *129*, 10551–10560.
- (28) Rzayev, J. Synthesis of polystyrene-polylactide bottlebrush block copolymers and their melt self-assembly into large domain nanostructures. *Macromolecules* **2009**, 42, 2135–2141.
- (29) Bolton, J.; Bailey, T. S.; Rzayev, J. Large pore size nanoporous materials from the self-assembly of asymmetric bottlebrush block copolymers. *Nano Letters* **2011**, *11*, 998–1001.
- (30) Gu, W.; Huh, J.; Hong, S. W.; Sveinbjornsson, B. R.; Park, C.; Grubbs, R. H.; Russell, T. P. Self-assembly of symmetric brush diblock copolymers. *ACS Nano* **2013**, *7*, 2551–2558.
- (31) Hong, S. W.; Gu, W.; Huh, J.; Sveinbjornsson, B. R.; Jeong, G.; Grubbs, R. H.; Russell, T. P. On the self-assembly of brush block copolymers in thin films. *ACS Nano* **2013**, *7*, 9684–9692.
- (32) Chremos, A.; Theodorakis, P. E. Morphologies of bottle-brush block copolymers. *ACS Macro Letters* **2014**, *3*, 1096–1100.
- (33) Gai, Y.; Song, D. P.; Yavitt, B. M.; Watkins, J. J. Polystyrene-block-poly(ethylene oxide) Bottlebrush Block Copolymer Morphology Transitions: Influence of Side Chain Length and Volume Fraction. *Macromolecules* **2017**, *50*, 1503–1511.
- (34) Lu, Y.; Larock, R. Novel Polymeric Materials from Vegetable Oils and Vinyl Monomers: Preparation, Properties, and Applications. *ChemSusChem* **2009**, 2, 136–147.
- (35) Hernández, N.; Williams, R. C.; Cochran, E. W. The battle for the "green" polymer.

- Different approaches for biopolymer synthesis: bioadvantaged vs. bioreplacement. *Organic & biomolecular chemistry* **2014**, *12*, 2834–49.
- (36) Yan, M.; Huang, Y.; Lu, M.; Lin, F.-Y.; Hernández, N. B.; Cochran, E. W. Gel Point Suppression in RAFT Polymerization of Pure Acrylic Cross-Linker Derived from Soybean Oil. *Biomacromolecules* **2016**, *17*, 2701–2709.
- (37) Yan, M.; Lin, F. Y.; Cochran, E. W. Dynamics of hyperbranched polymers derived from acrylated epoxidized soybean oil. *Polymer* **2017**, *125*, 117–125.
- (38) Chen, C.; Podolsky, J. H.; Hernandez, N.; Hohmann, A.; Williams, R. C.; Cochran, E. W. Use of Bioadvantaged Materials for Use in Bituminous Modification. *Transportation Research Procedia* **2016**, *14*, 3592–3600.
- (39) Chen, C.; Podolsky, J. H.; Williams, R. C.; Cochran, E. W. Determination of the optimum polystyrene parameters using asphalt binder modified with poly(styrene-acrylated epoxidised soybean oil) through response surface modelling. *Road Materials and Pavement Design* **2019**, 20, 572–591.
- (40) Haley, N. F.; Fichtner, M. W. Efficient and general synthesis of 1,3-dithiole-2-thiones. *The Journal of Organic Chemistry* **1980**, *45*, 175–177.
- (41) Mango, L. A.; Lenz, R. W. Hydrogenation of unsaturated polymers with diimide. *Die Makromolekulare Chemie* **1973**, *163*, 13–36.
- (42) Dae Han, C.; Kim, J. K. On the use of time-temperature superposition in multicomponent/multiphase polymer systems. *Polymer* **1993**, *34*, 2533–2539.
- (43) Ilavsky, J.; Jemian, P. R.; Allen, A. J.; Zhang, F.; Levine, L. E.; Long, G. G. Ultra-small-angle X-ray scattering at the Advanced Photon Source. *Journal of Applied Crystallog-raphy* **2009**, *42*, 469–479.

- (44) Ilavsky, J.; Jemian, P. R. <i>Irena</i>: tool suite for modeling and analysis of small-angle scattering. *Journal of Applied Crystallography* **2009**, 42, 347–353.
- (45) Zhang, F.; Ilavsky, J.; Long, G. G.; Quintana, J. P. G.; Allen, A. J.; Jemian, P. R. Glassy Carbon as an Absolute Intensity Calibration Standard for Small-Angle Scattering. *Metallurgical and Materials Transactions A* **2010**, *41*, 1151–1158.
- (46) Krigeaum, W. R.; Geymer, D. O. Thermodynamics of Polymer Solutions. The Polystyrene-Cyclohexane System near the Flory Theta Temperature. *Journal of the American Chemical Society* **1959**, *81*, 1859–1868.
- (47) Han, C. D.; Kim, J. K.; Kim, J. K. Determination of the Order—Disorder Transition Temperature of Block Copolymers. *Macromolecules* **1989**, 22, 383–394.
- (48) Libera, M. R.; Egerton, R. F. Advances in the transmission electron microscopy of polymers. *Polymer Reviews* **2010**, *50*, 321–339.
- (49) Khandpur, A. K.; Förster, S.; Bates, F. S.; Hamley, I. W.; Ryan, A. J.; Bras, W.; Almdal, K.; Mortensen, K. Polyisoprene-Polystyrene Diblock Copolymer Phase Diagram near the Order-Disorder Transition. *Macromolecules* **1995**, *28*, 8796–8806.
- (50) Arevalillo, A.; Muñoz, M. E.; Santamaría, A.; Fraga, L.; Barrio, J. A. Novel rheological features of molten SEBS copolymers: Mechanical relaxation at low frequencies and flow split. *European Polymer Journal* **2008**, *44*, 3213–3221.
- (51) Podzimek, S.; Vlcek, T. o. b. p. b. s. e. c. c. w. m. l. s. d. I. S. e. c. e. b. o. b. p.; Johann, C. Characterization of branched polymers by size exclusion chromatography coupled with multiangle light scattering detector. I. Size exclusion chromatography elution behavior of branched polymers. *Journal of Applied Polymer Science* **2001**, *81*, 1588–1594.

- (52) Meher, L.; Vidya Sagar, D.; Naik, S. Technical aspects of biodiesel production by transesterification—a review. *Renewable and Sustainable Energy Reviews* **2006**, *10*, 248–268.
- (53) Leibler, L. Theory of Microphase Separation in Block Copolymers. *Macromolecules* **1980**, *13*, 1602–1617.
- (54) Olmsted, P. D.; Milner, S. T. Strong Segregation Theory of Bicontinuous Phases in Block Copolymers. *Macromolecules* **1998**, *31*, 4011–4022, Publisher: American Chemical Society.
- (55) Grason, G. M.; Kamien, R. D. Self-consistent field theory of multiply branched block copolymer melts. *Physical Review E* **2005**, *71*, 051801, Publisher: American Physical Society.
- (56) Matsushita, Y.; Takasu, T.; Yagi, K.; Tomioka, K.; Noda, I. Preparation and morphologies of 4- and 12-armed styrene-isoprene star-shaped block copolymers. *Polymer* **1994**, *35*, 2862–2866.
- (57) Xu, Y.; Li, W.; Qiu, F.; Lin, Z. Self-assembly of 21-arm star-like diblock copolymer in bulk and under cylindrical confinement. *Nanoscale* **2014**, *6*, 6844–6852.
- (58) Valerie Grayer, E. E., Dormidontova; Hadziioannou, G. A Comparative Experimental and Theoretical Study between Heteroarm Star and Diblock Copolymers in the Microphase Separated State. *Macromolecules* **2000**, *33*, 6330–6339.
- (59) Georgopanos, P.; Lo, T.-Y.; Ho, R.-M.; Avgeropoulos, A. Synthesis, molecular characterization and self-assembly of (PS-b-PDMS) <sub>n</sub> type linear (n = 1, 2) and star (n = 3, 4) block copolymers. *Polym. Chem.* **2017**, *8*, 843–850.